

First-principles investigation of grain boundary structure effects on hydrogen solubility and segregation in tungsten

Wenhao He , Xing Gao , Liangfu Zhou , Dongyan Yang , Zhiguang Wang ,
Juntao Liu , Zhiyi Liu & Yuhong Li

To cite this article: Wenhao He , Xing Gao , Liangfu Zhou , Dongyan Yang , Zhiguang Wang , Juntao Liu , Zhiyi Liu & Yuhong Li (2020): First-principles investigation of grain boundary structure effects on hydrogen solubility and segregation in tungsten, Journal of Nuclear Science and Technology, DOI: [10.1080/00223131.2020.1816229](https://doi.org/10.1080/00223131.2020.1816229)

To link to this article: <https://doi.org/10.1080/00223131.2020.1816229>



Published online: 16 Sep 2020.



Submit your article to this journal



Article views: 51



View related articles



View Crossmark data

ARTICLE



First-principles investigation of grain boundary structure effects on hydrogen solubility and segregation in tungsten

Wenhai He^a, Xing Gao^b, Liangfu Zhou^a, Dongyan Yang^a, Zhiguang Wang^b, Juntao Liu^a, Zhiyi Liu^a and Yuhong Li^a

^aSchool of Nuclear Science and Technology, Lanzhou University, Lanzhou, China; ^bInstitute of Modern Physics, Chinese Academy of Sciences, Lanzhou, China

ABSTRACT

Hydrogen (H) solubility, segregation, and hydrogen-induced intergranular fractures in eight symmetric tilt grain boundaries (GBs) in tungsten (W) are investigated through the first-principles calculations. The results show that there is an equilibrium distance, about 1.95 Å, between the H inserted in interstitial sites and its nearest W. Interactions between the inserted H and GBs are rather localized, thus the local environments of interstitial sites are responsible for the hydrogen solubility. The hydrogen solution energy decreases as the hard-sphere radius r_0 of the interstitial site increases. But the trend slows significantly down as the r_0 is larger than 0.57 Å, which is corresponding to the equilibrium H-W distance of 1.95 Å, due to the ignorable contributions from lattice distortions induced by the inserted H to the hydrogen solution energy. It is found out that the GBs with smaller interstitial site are more resistant to hydrogen segregation as well as the hydrogen-induced intergranular fractures. Among all GBs studied here, the twin GB $\Sigma 3(110)[111]$ has the smallest interstitial site; hence, it has the weakest capability to trap H and it is also the most resistant to hydrogen-induced intergranular fractures. Our results provide a sound guide to design GBs to suppress hydrogen-induced intergranular fractures.

ARTICLE HISTORY

Received 15 April 2020

Accepted 25 August 2020

KEYWORDS

Tungsten; grain boundary; hydrogen solution; intergranular fractures; first-principles

1 Introduction

The doping of foreign elements created by nuclear reactions between projectile particles and material atoms is an important aspect of macroscopic radiation damage effects on materials served in nuclear devices [1,2]. One of the widely concerned foreign elements is hydrogen (H) [3–11], which is abundant in manufacturing processes and service environments. It is well known that grain boundaries (GBs) can act as the sink for point defects, such as H, helium, vacancies, and self-interstitial atoms [12–16]. Therefore, GBs can effectively enhance the annihilation of the vacancies and self-interstitial atoms. That is, GBs can improve the irradiation resistance of materials. However, in metallic systems, segregation of H in GBs often embrittles the materials by causing a sharp transition from ductile fracture to brittle intergranular fracture accompanied by a drastic loss in toughness and ductility [3–6], which is called hydrogen embrittlement (HE). It has been experimentally demonstrated that solubility and segregation of H in GBs are sensitive to the characters of GBs. A recent experiment conducted by Bechtle *et al.* showed that the HE resistance of nickel could be drastically increased by increasing fractions of ‘special GBs’ that were characterized with low excess free volumes and high degree of atomic matching [6]. A possible reason is that the random GBs

have a higher segregation ability for H than the ‘special GBs.’ Hence the hydrogen concentration is higher in random GBs than that in the ‘special GBs’ [6]. In addition, the investigation conducted by Oudriss *et al.* showed that some special GBs with high dislocation density could trap hydrogen atoms and slow down hydrogen diffusions [17]. These studies pointed out that the hydrogen segregation, diffusion, and embrittlement depend on the GB structures and suggested that the possibility of enhancing the HE resistance of materials through GB engineering. Therefore, it is of fundamental importance to further explore relationships of the H solubility and segregation in GBs on the structures of the GBs on atomic scales.

Tungsten (W) and its alloys are considered to be promising candidates for plasma-facing materials (PFMs), such as the first wall materials and divertor of the magnetic confinement fusion reactor, due to their high melting temperature, high thermal conductivity, and low sputtering erosion [18,19]. The PFMs will be exposed to extremely high fluxes of H isotope (deuterium-tritium) ions [20]. Simulation results using both density functional theory (DFT) and molecular dynamics (MD) have indicated that GBs can play as trapping centers for the H; thus, the H strongly segregates to the GBs in W [13–16], which is in agreement

with experimental observations. It is worthwhile to mention that these DFT simulations about the H solubility and segregation in GBs in W were only based on some special GBs. For example, Zhou *et al.* studied the H solubility and diffusion in GB $\Sigma 5(310)[001]$ [13], Xiao *et al.* focused to the H trapping in GB $\Sigma 3(111)[110]$, [14], while Gonzalez *et al.* investigated the H trapping and mobility in a non-coherent (110)/(112) interface [16]. The hydrogen segregation energies are respectively -1.11 eV, -1.31 eV and -1.15 eV in the most stable interstitial sites in GB $\Sigma 5(310)[001]$, [13], GB $\Sigma 3(111)[110]$, [14] and non-coherent (110)/(112) interface [16]. Obviously, the hydrogen segregation energy indeed depends on the GB structures. In addition, Goto J. *et al.* also calculated the hydrogen segregation energy in GB $\Sigma 3(111)[110]$, and the final result was -0.97 eV [21], which differed from -1.31 eV obtained in reference [14] due to the differences in calculation methods. Therefore, it is essential to employ same method to investigate the hydrogen solubility and segregation in different GBs in W, especially the dependences of hydrogen solubility on the microstructures of GBs.

This paper aims to systematically study the H solubility and segregation in GBs in W. Eight symmetric tilt GBs constructed by the coincidence site lattice (CSL) model [22] are selected to carry out this investigation. Both the interstitial sites in GBs and in bulk are identified by convex deltahedra. The lattice distortions and charge density changes induced by the inserted H are analyzed. The hydrogen solution energies in each interstitial site in the eight GBs are computed through the first-principles total energy calculations. The effects of GB structures on the hydrogen solution energy are analyzed. In addition, combined the thermodynamic Rice-Wang mode, hydrogen-induced intergranular fractures of various GBs studied here are discussed.

2 Structural models and computational details

First-principles total energy calculations [23] were carried out with the Vienna Ab initio Simulation Package (VASP) [24–26] based on the DFT [27,28]. The projected augmented wave (PAW) [25] pseudo-potentials were employed in the all calculations within the generalized gradient approximation (GGA) with Perdew and Wang [29] functional for the exchange and correlation energies. The detailed methods employed to calculate the total energy of systems in this study are the same with those used in our previous studies, in which the influence of the GBs characters on helium solubility and segregation [30], vacancy and self-interstitial atoms [31] have been investigated in W. Since the H atom is a light-mass particle and therefore has a high vibrational energy compared to the relatively slowly moving heavy metal atoms, the

zero-point energy of H has been taken into account by summing up the zero-point vibrational energies of hydrogen normal modes.

Similar to our previous investigations [30,31], eight symmetric tilt GBs, $\Sigma 3(110)[111]$, $\Sigma 3(111)[110]$, $\Sigma 5(310)[001]$, $\Sigma 5(210)[001]$, $\Sigma 9(114)[110]$, $\Sigma 11(332)[110]$, $\Sigma 17(410)[001]$, and $\Sigma 19(116)[110]$ were constructed by the CSL model [22], and the interstitial sites were identified with convex deltahedra in this study. There are five types of convex deltahedron, tetrahedron (TET), octahedron (OCT), pentagonal bipyramid (PBP), cap trigonal prism (CTP), and bitemrahedron (BTE) in these eight GBs studied here. The detailed schemes of constructing GBs and identifying interstitial sites in these GBs were elaborated in our previous studies [30,31].

To calculate work of separation of a GB, the GB is generally separated into two parts. Currently, two different methods are widely used to simulate the separation of GBs. One, successively increasing the tensile stress for the initial GB system until it separates into two parts. This method can ensure the GB system to separate along the path with the lowest binding energy. It is also the closest process to the actual separation of a GB. However, this method is always time consuming, and the atomic relaxation is hard to converge in strain field [32]. Second, the GB system are initially separated into two parts along the possible paths, which is a time-saving method. Nickel GB tension simulation has shown that the results obtained with these two schemes are identical [33]. Therefore, to save time, the second method is employed in this study. As an example, the separated model of GB $\Sigma 5(310)[001]$ is shown in Figure 1. The GB system separates into two free surface (FS) systems and each FS system has two different surfaces. A vacuum layer has to be added into the FS system to eliminate interactions between these two surfaces. The total energy convergence of FS system was checked with different thickness of vacuum layer and a 10 \AA vacuum layer is enough to eliminate the interactions between these two surfaces. When the GB systems contained a H atom are separated into two FSs, the H atom is also assigned to one of the FS systems and its position is allowed to relax freely.

The hydrogen solution energies in GBs and bulk were calculated to investigate the H solubility in GBs in this study. In order to combine the thermodynamic Rice-Wang mode [34] to study the effects of H segregation in GBs on hydrogen-induced intergranular fractures, the hydrogen solution energies at the FSs were also calculated. The hydrogen solution energy $E_{GB(FS,bulk),H}^{S,i}$ in the i^{th} kind of interstitial site in a GB, FS, and bulk can be calculated by

$$E_{GB(FS,bulk),H}^{S,i} = E_{GB(bulk),H}^{Def,i} - E_{GB(FS,bulk)}^{Perf} - \frac{E_{H_2}}{2} \quad (1)$$

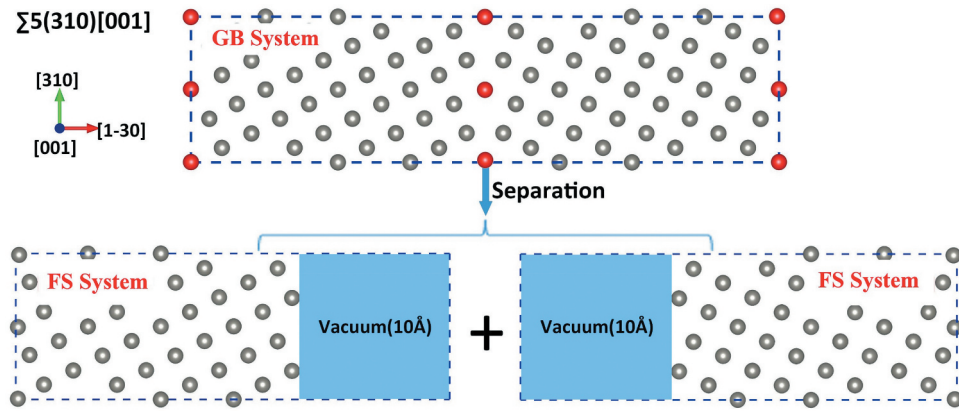


Figure 1. Schematic illustration of GB $\Sigma 5(310)[001]$ separation.

where $E_{GB(FS,bulk),H}^{Def,i}$ is the total energy of the supercell with a hydrogen atom in the i^{th} kind of interstitial site in the GB (FS, bulk), $E_{GB(FS,bulk)}^{\text{Perf}}$ is the total energy of the supercell containing clean GB (FS, bulk), and E_{H_2} is the energy of a hydrogen molecule in vacuum. In this study, a $10 \text{ \AA} \times 10 \text{ \AA} \times 10 \text{ \AA}$ supercell containing one hydrogen molecule was used to calculate E_{H_2} . A $4 \times 4 \times 4$ supercell (128 atoms) was constructed with the calculated lattice parameter of 3.19 \AA to compute the hydrogen solution energies in TET and OCT interstitial sites in the bulk.

The hydrogen segregation energy $E_{GB(FS),H}^{\text{seg},i}$ in the i^{th} kind of interstitial site in a GB (FS) is defined as

$$E_{GB(FS),H}^{\text{seg},i} = E_{GB(FS),H}^{S,i} - E_{bulk,H}^S, \quad (2)$$

where $E_{GB(FS),H}^{S,i}$ is the hydrogen solution energy in the i^{th} kind of interstitial site in the GB (FS) and $E_{bulk,H}^S$ is the lowest hydrogen solution energy in bulk W. In line with previous investigations [35–38], our calculated hydrogen solution energy in TET interstitial site is lower than that in OCT interstitial site in bulk W. Therefore, $E_{bulk,H}^S$ is the hydrogen solution energy in TET interstitial site in bulk W.

The segregation of hydrogen atoms in GBs will degrade intergranular fracture strength, which can be characterized by the work of separation of GBs containing hydrogen atoms. Combined first-principles calculations with the thermodynamic Rice-Wang mode [34], the work of separation W_c of GB containing hydrogen atoms can be obtained as follows:

$$W_c \approx W_0 - \sum_i (E_{GB,H}^{\text{seg},i} - E_{FS,H}^{\text{seg},i}) * c_i * \theta_i, \quad (3)$$

where W_0 is the work of separation for clean GB without any hydrogen atom, c_i is the equilibrium hydrogen concentration in the i^{th} kind of interstitial site, and θ_i is the density of the i^{th} kind of interstitial site in GB plane. The c_i can be determined by [39,40]

$$\frac{c_i}{1 - c_i} = \frac{c_0}{1 - c_0} * \exp\left(-\frac{E_{GB,H}^{\text{seg},i}}{K_B * T}\right), \quad (4)$$

where c_0 is the equilibrium hydrogen concentration (defined as the H/W atomic ratio) in an unstressed bulk crystal, K_B is the Boltzmann constant, and T is the temperature. The work of separation W_0 of a clean GB can be defined as follows:

$$W_0 = \frac{2 * E_{FS} - E_{GB}^{\text{Perf}}}{2 * S} \quad (5)$$

where E_{FS} is the total energy of a FS system, E_{GB}^{Perf} is the total energy of GB system, and S is the cross-section area of the GB.

It is noted that the equations (3) and (4) are reasonable for dilute limits of non-interacting H. The hydrogen concentration c_i in GBs is higher than bulk c_0 . Taking CTP interstitial sites in GB $\Sigma 11(332)[110]$ as an example, the interaction between two hydrogen atoms inserted into the nearest CTP interstitial sites in GB $\Sigma 11(332)[110]$ has been calculated. It is found out that the interaction energy between them is very small, which is about 0.08 eV. Therefore, we assume that using the equations (3) and (4) as an approximate model to estimate the hydrogen concentration as well as the work of separation of GBs with H may be reasonable in this study.

3 Results and discussions

3.1. Charge density differences

Charge density differences with and without H in GBs are analyzed after relaxations. As defined in the references [41,42], the charge density change is defined as the charge density of GB systems with a hydrogen atom subtracts that of the pure GB systems and then subtracts that of a hydrogen atom in vacuum. As an example, the charge density changes for TET and CTP

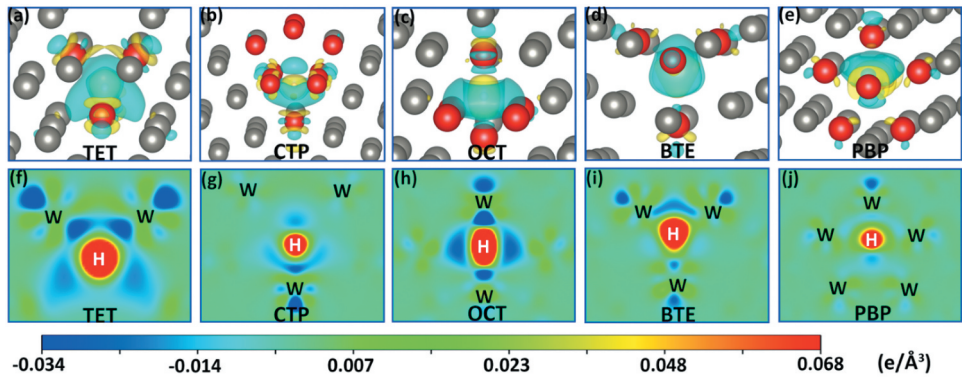


Figure 2. Three-dimensional charge density differences for TET and CTP in GB $\Sigma 5(310)[001]$, and OCT, BTE, and PBP in GB $\Sigma 9(114)[110]$.

in GB $\Sigma 5(310)[001]$ and OCT, BTE, and PBP in GB $\Sigma 9(114)[110]$ are shown in Figure 2. Similar results are observed for other interstitial sites in all other GBs studied here. Three-dimensional charge density differences are shown from (a) to (e), and two-dimensional charge density differences along (001) plane containing the H are shown from (f) to (j) for these five types of polyhedral interstitial sites, respectively. In general, the charge density at the H site greatly increases for all interstitial sites studied here. It shows that the H picks up electrons from its surrounding environments due to its open-shelled electronic structure. These phenomena agree with those reported in previous studies on single crystal tungsten and other metals [41,42]. In addition, it is found that the dominant change of the charge density occurs in regions around the interstitial site, that is, interactions between the H in interstitial sites and GBs are rather localized. Therefore, the hydrogen solution energy may be dominantly determined by the local environment of the interstitial sites.

3.2. Relationship between hydrogen solution energy and atomic distribution around interstitial site

Hydrogen solution energies E_H^S in all interstitial sites in GBs were calculated. Supercell size would affect the E_H^S due to the periodic boundary conditions. Therefore, the effects of supercell size on the E_H^S were checked for GB $\Sigma 11(332)[110]$ firstly, and the results are listed in Table 1. It is obvious that the difference of E_H^S obtained from different supercell sizes is minute, and the smaller supercell size is adequate to calculate the E_H^S for GB $\Sigma 11(332)[110]$. However, to obtain

more accurate results, the larger supercell size with 168 tungsten atoms is used for GB $\Sigma 11(332)[110]$ in this study. For other GBs, the supercell sizes along their shortest axis are larger than 5.26 Å. Hence, we assume that the supercell sizes for all GBs studied here are large enough to study the hydrogen solubility in GBs.

Hydrogen solution energies E_H^S in all interstitial sites in different GBs and in the bulk are listed in Table 2. The E_H^S is 0.91 eV and 1.29 eV in TET and OCT interstitial sites in bulk W respectively, which agrees with previously reported results of 1.08 eV and 1.48 eV [43]. It is implied that the H prefers to occupy the TET interstitial site in single-crystal tungsten. It is noted that some of E_H^S are negative, which shows that H will exothermically enter into these GBs with negative E_H^S . In general, the E_H^S in interstitial sites in GBs are smaller than that in TET interstitial site in bulk, showing that the H prefers to segregate to the GBs in W. In addition, the E_H^S are extremely different for various GBs, and even for the different interstitial sites in the same GB. It shows that the E_H^S is closely related to the local atomic distribution around interstitial site. As mentioned above, the charge density differences also demonstrate this conclusion. In order to reveal the atomic distribution around interstitial site effects on the E_H^S , the relationship between E_H^S and the hard-sphere radius r_0 of interstitial sites is shown in Figure 3(a) for all interstitial sites in GBs and in bulk. The r_0 is defined as the largest hard-sphere radius which can be inserted into the interstitial site.

The E_H^S firstly decreases as the hard-sphere radius r_0 of the interstitial site increases. It may be concluded that the H prefers to occupy the larger interstitial sites

Table 1. Hydrogen solution energies E_H^S calculated with different supercell sizes for GB $\Sigma 11(332)[110]$.

GB systems	Number of atoms	k -mesh	L_a (Å)	L_b (Å)	L_c (Å)	Interstitial Sites	E_H^S (eV)
$\Sigma 11(332)[110]$	84	1*5*3	29.12	5.26	9.03	CTP	0.26
$\Sigma 11(332)[110]$	168	1*3*3	29.10	10.53	9.03	CTP	0.23
$\Sigma 11(332)[110]$	84	1*5*3	29.12	5.26	9.03	BTE	0.84
$\Sigma 11(332)[110]$	168	1*3*3	29.10	10.53	9.03	BTE	0.78

Table 2. Hard-sphere radii r_0 , hydrogen solution energies E_H^S , mechanical contributions E_H^{MC} and chemical contributions E_H^{CC} to E_H^S for all interstitial sites in the eight GBs studied here and in bulk.

Systems	Interstitial sites	r_0 (Å)	E_H^S (eV) This work (Ref.)	E_H^{MC} (eV)	E_H^{CC} (eV)
Bulk	TET	0.40	0.99 (1.08 ^a)	0.20	0.79
	OCT	0.21	1.39 (1.48 ^a)	0.42	0.96
$\Sigma 3(110)[111]$	OCT1	0.57	0.29	0.07	0.22
	OCT2	-0.01	2.33	0.73	1.60
$\Sigma 3(111)[110]$	CTP	0.72	0.07	0.02	0.05
	CTP	0.95	-0.08	0.06	-0.14
$\Sigma 5(210)[001]$	TET	0.40	0.22	0.24	-0.02
	CTP	0.87	0.01	0.07	-0.06
	BTE	0.33	0.32	0.15	0.17
$\Sigma 9(114)[110]$	PBP	0.44	0.34	0.22	0.12
	PBP	0.86	-0.10	0.02	-0.12
	BTE	0.33	0.63	0.27	0.36
$\Sigma 11(332)[110]$	OCT	-0.05	1.64	0.83	0.81
	CTP	0.60	0.23	0.04	0.19
$\Sigma 17(410)[001]$	BTE	0.34	0.78	0.22	0.56
	CTP1	0.94	-0.17	0.03	-0.20
	CTP2	1.00	-0.27	0.02	-0.29
$\Sigma 19(116)[110]$	TET1	0.40	0.30	0.29	0.01
	TET2	0.35	0.95	0.29	0.65
	CTP	1.09	-0.08	0.01	-0.09
	PBP	0.72	0.05	0.11	-0.06

(^a [45])

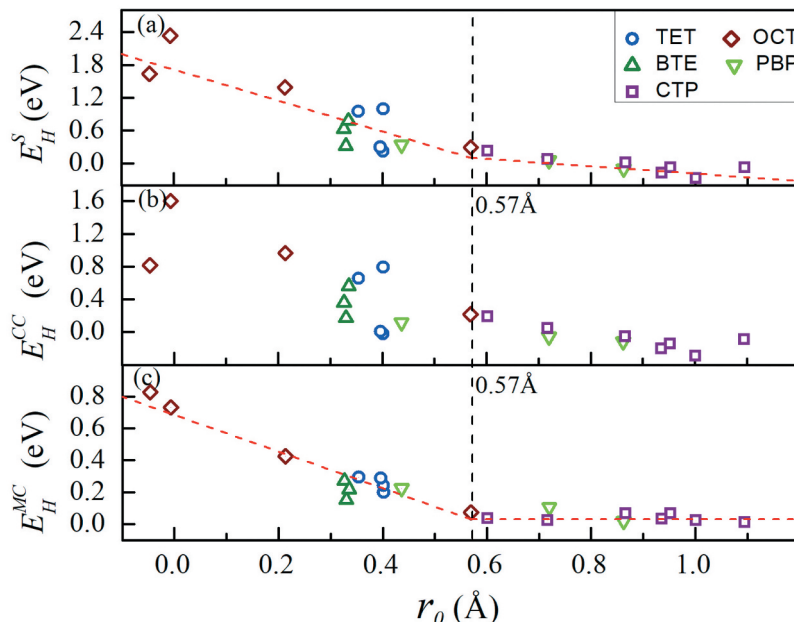


Figure 3. Hydrogen solution energies E_H^S , mechanical contribution E_H^{MC} as well as chemical contribution E_H^{CC} to E_H^S versus hard-sphere radius r_0 of interstitial sites.

in W. As the r_0 reaches 0.57 Å, the trend of this variation significantly slows down. In order to further understand this relationship, the hydrogen solution energy E_H^S is divided into two parts, chemical contribution E_H^{CC} and mechanical contribution E_H^{MC} , according to the methods reported in references [44,45]. The E_H^{CC} is caused by direct electronic interaction and redistribution of the charge density induced by the inserted H [45]. The E_H^{MC} is attributed to the lattice deformation due to the inserted H [45]. The chemical contribution E_H^{CC} and the mechanical contribution

E_H^{MC} versus the hard-sphere radius r_0 of interstitial site are shown in Figure 3(b) and (c), respectively. In addition, the E_H^{CC} is larger than E_H^{MC} for all interstitial sites, which indicates that the chemical contribution for hydrogen solution energy is larger than mechanical contribution. The chemical contribution E_H^{CC} always decreases as the r_0 increases. However, the E_H^{MC} firstly decreases as the r_0 increases, and then keeps near zero as the r_0 is larger than 0.57 Å. Thus, the main reason for the slowdown in variation tendency of E_H^S with r_0 when r_0 is larger than 0.57 Å is that the E_H^{MC} keep

about zero. To further explain the phenomenon, the changes of structure induced by the inserted H are discussed in the next section.

3.3. Structural relaxation

After H atom was initially introduced in the center of interstitial sites in bulk and GBs, both atomic positions and volumes of the bulk and GB systems were relaxed. The distances from the H to its first nearest W are defined as d_{H-W}^{unrel} for unrelaxed system, and d_{H-W}^{rel} for relaxed system, respectively. After relaxation, the change Δd of the distance from H to its first nearest W is thus defined as

$$\Delta d = d_{H_W}^{rel} - d_{H_W}^{unrel} \quad (6)$$

In Figure 4(a), the Δd versus the d_{H-W}^{unrel} for all interstitial sites are plotted. Clearly, the Δd decreases as the d_{H-W}^{unrel} increases. When the d_{H-W}^{unrel} is smaller than 1.95 Å, the Δd is positive, showing that the distance from H to its first nearest W increases after relaxations. In contrast, the Δd is negative when d_{H-W}^{unrel} is larger than 1.95 Å, showing that the distance from H to its first nearest W decreases after relaxations. As the d_{H-W}^{unrel} is smaller than 1.95 Å, the relaxed atomic configurations show that the outward movements of the W atoms around interstitial sites result in the increase of the distances between H and its first nearest W. Moreover, the smaller the d_{H-W}^{unrel} is, the larger the Δd is. For interstitial sites with the d_{H-W}^{unrel} larger than 1.95 Å, the decrease of the distance between the H and its first nearest W should be attributed to the movement of H to one of its surrounding W atoms which almost stay still during relaxation. As an example, the unrelaxed and relaxed atomic distributions of CTP

interstitial site with d_{H-W}^{unrel} of 2.33 Å in GB Σ5(310)[001] are also shown in Figure 4(c) and (d). The changes in distances between the center of CTP and its neighboring atoms are ignorable compared to the distance, about 1.36 Å, that H moves. The phenomenon is similar to that observed in other interstitial sites with d_{H-W}^{unrel} larger than 1.95 Å. This shows that the decrease of the distance between the H and its first nearest W should be attributed to the movement of H to one of its surrounding W atoms rather than the movement of host atoms for interstitial sites with the d_{H-W}^{unrel} larger than 1.95 Å.

As mentioned above, the distance from H to its first nearest W increases during relaxations due to the movement outward of the nearest host atom for the interstitial sites in which the distance from H to its first nearest W is smaller than 1.95 Å initially. The distance from H to its first nearest W decreases during relaxations due to the movement of the hydrogen atom for the interstitial sites in which the distance from H to its first nearest W is larger than 1.95 Å initially. Thus, it may be a reasonable assumption that there is an equilibrium distance, about 1.95 Å, between the H in interstitial site and its first nearest W. To further verify this assumption, the relation between $d_{H_W}^{rel}$ and $d_{H_W}^{unrel}$ is shown in Figure 4 (b). It is obvious that the $d_{H_W}^{rel}$ firstly increases as the $d_{H_W}^{unrel}$ increases and keeps about 1.95 Å for the interstitial sites in which the $d_{H_W}^{unrel}$ is larger than 1.95 Å initially, which further demonstrates the conclusion that the equilibrium distance between the H in interstitial site and its first nearest W is about 1.95 Å. This equilibrium H-W distance agrees with the distance of 1.92 Å between H and its nearest host atom at W(100) and W(110) surfaces calculated from DFT simulations

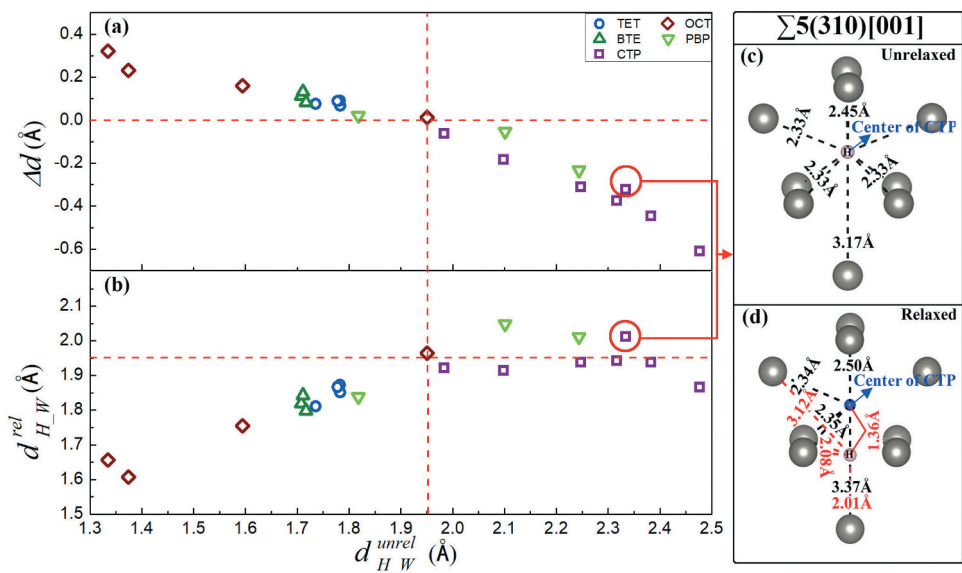


Figure 4. After relaxation the distance change Δd and the distance d_{H-W}^{rel} from H to its first nearest W vs. the H-W distance d_{H-W}^{unrel} for unrelaxed atomic configuration.

[46], and the distance obtained from experimental measurement, 1.9 Å, between H and W surfaces [47].

The interstitial sites with the equilibrium distance of 1.95 Å between H and its nearest W corresponds to the hard-sphere radius r_0 of 0.57 Å. For the interstitial sites with r_0 lesser than 0.57 Å, in order to enlarge the distance between the hydrogen atom and the nearest host atom to 1.95 Å, the host atoms around interstitial site have to move outward. The smaller the r_0 is, the more the distance that the host atoms move outward, the more the deformation of the interstitial sites. Therefore, the E_H^{MC} decreases as the r_0 increases. However, the host atoms around interstitial site do not need to move outward for the r_0 larger than 0.57 Å, because the distance between the hydrogen atom and the nearest host atom is larger than 1.95 Å for the initial interstitial sites, and only a movement of hydrogen atom will ensure the distance between them becomes about 1.95 Å. Therefore, the E_H^{MC} becomes about zero when the r_0 is larger than 0.57 Å.

3.4. Hydrogen segregation in GBs

Hydrogen segregation energy $E_{GB,H}^{\text{seg},i}$ in the i^{th} kind of interstitial site in GB can be obtained from equation (2). The $E_{GB,H}^{\text{seg},i}$ varies for different kinds of interstitial site in the same GB due to the different solution energies $E_{GB,H}^S$. Since the H prefers to occupy the interstitial site with the smallest segregation energy, the smallest $E_{GB,H}^{\text{seg},i}$ in a GB is defined as the hydrogen segregation energy $E_{GB,H}^{\text{seg}}$ in the GB. The same method has been applied to investigate the segregation of helium atom, vacancy, and self-interstitial atom in GBs in W in our previous studies [30,31]. As mentioned above, the $E_{GB,H}^S$ decreases as the hard-sphere radius r_0 of the interstitial site increases, hence, the $E_{GB,H}^{\text{seg}}$ will also decrease as the r_0 increases according to

equation (2). Thus, the H prefers to segregate to the larger interstitial sites in GBs. The hydrogen segregation energies $E_{GB,H}^{\text{seg}}$ in GB $\Sigma 3(110)[111]$ and $\Sigma 5(310)[001]$ in this study and reference [13,48] are compared in Table 3. Although the potential types and numbers of atom contained in simulation cells are different in this study and references [13,48], the final $E_{GB,H}^{\text{seg}}$ are approximately equal, which further demonstrates that GB structures and calculation parameters used in this study are reasonable.

The hydrogen segregation energies $E_{GB,H}^{\text{seg}}$ as well as the hard-sphere radius r_0 of the largest interstitial site in each GB studied here are listed in Table 4. Obviously, the $E_{GB,H}^{\text{seg}}$ in GB $\Sigma 3(110)[111]$ is the largest among all GBs studied here, which means that the GB $\Sigma 3(110)[111]$ is the most resistant to the H segregation. This is because the GB $\Sigma 3(110)[111]$ has the smallest interstitial site among GBs studied here.

To further verify the results mentioned above, hydrogen concentrations c_i in the i^{th} interstitial site in GBs were calculated according to equation (4). The larger the interstitial site is, the smaller the $E_{GB,H}^{\text{seg},i}$ in the interstitial site in GB is, hence, according to equation (4) the c_i is larger in the interstitial site with larger hard-sphere radius r_0 . In addition, the c_i in the largest interstitial site is far higher than that in other interstitial sites in the same GB due to the significant difference between the hydrogen segregation energy. For example, the c_i is about 6.78×10^{-2} in CTP and 1.20×10^{-5} in BTE in GB $\Sigma 11(332)[110]$ as the equilibrium hydrogen concentration c_0 in bulk is 10^{-5} and the temperature is 1000 K. Therefore, for each GB only the largest interstitial site was considered to calculate the hydrogen concentration c_i in GBs. Taking temperature of 1000 K, which is the typical service temperature of the plasma-oriented materials in a fusion environment [49], as an example, for all GBs studied

Table 3. Hydrogen segregation energies $E_{GB,H}^{\text{seg}}$ into GB $\Sigma 3(110)[111]$ and $\Sigma 5(310)[001]$, numbers of atoms contained in simulation cells as well as potential types in this study and reference.

GB systems	Potential types	This work (reference)	Numbers of atoms	This work (reference)	$E_{GB,H}^{\text{seg}}$ (eV)	This work (reference)
$\Sigma 3(110)[111]$	PW (PBE ^a)		160 (80 ^a)		-0.70 (-0.64 ^a)	
$\Sigma 5(310)[001]$	PW (PW ^b)		144 (138 ^b)		-1.07 (-1.11 ^b)	

(^a [48], ^b [13])

Table 4. Hard-sphere radii r_0 of the largest interstitial site and hydrogen segregation energies $E_{GB,H}^{\text{seg}}$ in the eight symmetric tilt GBs studied here.

GB systems	The largest interstitial site (r_0 (Å))	$E_{GB,H}^{\text{seg}}$ (eV) This work	GB systems	The largest interstitial site (r_0 (Å))	$E_{GB,H}^{\text{seg}}$ (eV) This work
$\Sigma 3(110)[111]$	OCT1 (0.57)	-0.70	$\Sigma 9(114)[110]$	PBP (0.86)	-1.09
$\Sigma 11(332)[110]$	CTP (0.60)	-0.77	$\Sigma 5(310)[001]$	CTP (0.95)	-1.07
$\Sigma 3(111)[110]$	CTP (0.72)	-0.92	$\Sigma 19(116)[110]$	CTP (1.09)	-1.07
$\Sigma 5(210)[001]$	CTP (0.87)	-0.98	$\Sigma 17(410)[001]$	CTP2 (1.00)	-1.26

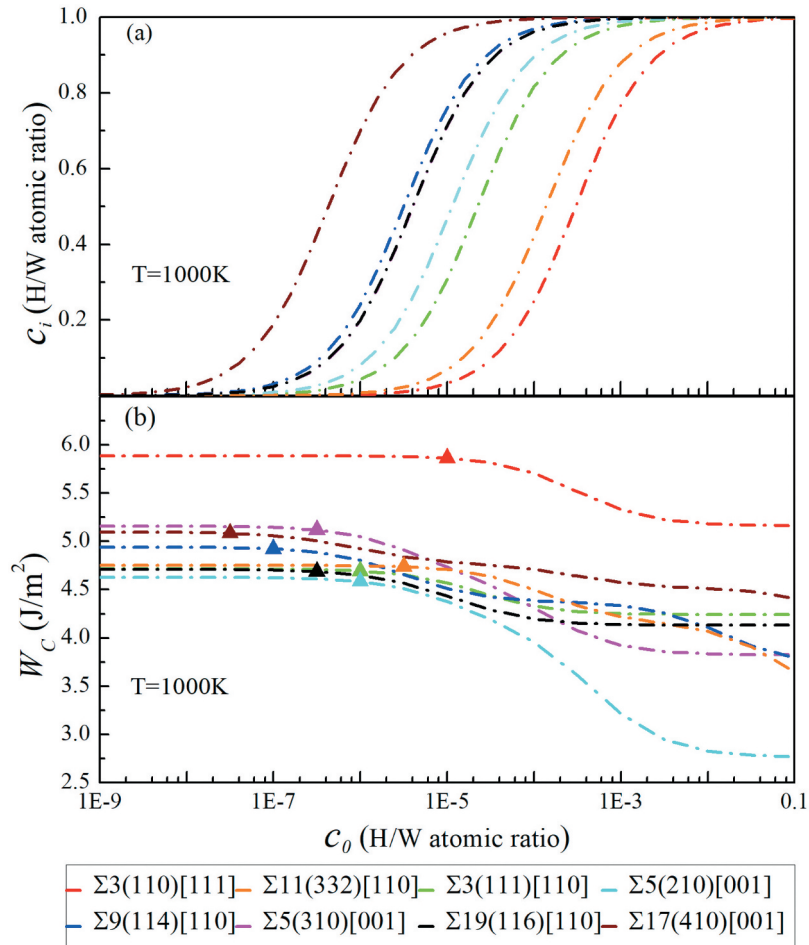


Figure 5. Hydrogen concentration c_i in the largest interstitial sites in GBs as well as work W_c of separation of GB with hydrogens vs. equilibrium hydrogen concentration c_0 in bulk.

here the relationships between c_i and c_0 are shown in Figure 5(a). For other temperatures, the result is similar to that at 1000 K.

In general, the c_i increases as the c_0 increases for each GB. However, the c_i begin to increase remarkably at different C_0 for various GBs. For GB $\Sigma 17(410)[001]$, the c_i starts to increases sharply as the c_0 is about 3.16×10^{-8} , then the c_i in GB $\Sigma 19(116)[110]$, $\Sigma 5(310)[001]$, $\Sigma 9(114)[110]$ etc increase markedly in turn as the c_0 increases. For twin GB $\Sigma 3(110)[111]$, the c_i starts to increase significantly until the c_0 is about 1×10^{-5} , which means that the GB $\Sigma 3(110)[111]$ is really the most resistant to the H segregation compared to other GBs studied here under the same c_0 . It can be attributed to the smallest interstitial site in GB $\Sigma 3(110)[111]$ among all GBs studied here.

3.5. Effects of hydrogen segregations on intergranular fracture

Hydrogen segregation in GBs usually degrades the fracture strength of GBs, which can be characterized by the work of GB separation. To investigate the effects of H segregation in different GBs on the fracture strength, firstly the work of separation W_0 of clean GBs studied here were calculated with equation (5). The results are listed in Table 5. Clearly, the W_0 of GB $\Sigma 3(111)[110]$ in this study and that reported in references [50] are consistent. Compared to the work of separation 7.07 J/m^2 of single-crystal W reported in reference [50], the W_0 of GBs are largely reduced. This is because that lattice deformations of GBs decrease the cohesive energy. The W_0 of GB $\Sigma 3(110)[111]$ is

Table 5. Work of separation W_0 of clean GBs studied here.

GBs	W_0 (J/m^2)	GBs	W_0 (J/m^2)	GBs	W_0 (J/m^2)
$\Sigma 3(110)[111]$	5.89	$\Sigma 5(310)[001]$	5.16	$\Sigma 3(111)[110]$	4.72 (4.77 ^a)
$\Sigma 5(210)[001]$	4.63	$\Sigma 11(332)[110]$	4.75	$\Sigma 19(116)[110]$	4.71
$\Sigma 9(114)[110]$	4.94	$\Sigma 17(410)[001]$	5.10		

^a [50]

5.89 J/m², which is the largest among all the GBs studied here due to the slightest lattice deformation.

Based on the calculated work W_0 of clean GBs separation above, the work of separation W_c of GBs containing the H atoms was obtained via equation (3). In this study, taking temperature 1000 K as an example, the relationship between W_c and the equilibrium hydrogen concentration C_0 in bulk for all GBs studied here are shown in Figure 5(b). There are similar results at other temperatures. Clearly, the work of separation W_c decreases as c_0 increases for all GBs. As the c_0 is very low (e.g. less than 10^{-9}), the W_c are equal to the work of separation W_0 corresponding to clean GBs since the hydrogen concentration c_i in GB is almost zero. It is noted that the W_c of different GBs start to markedly decrease at different c_0 . For GB $\Sigma 17(410)[001]$, the W_c starts to dramatically decreases as the c_0 is about 3.16×10^{-8} . Then the W_c of GB $\Sigma 19(116)[110]$, GB $\Sigma 5(310)[001]$, GB $\Sigma 9(114)[110]$ etc markedly decline in turn as the c_0 increases. Compared to the relationships between c_i and C_0 shown in Figure 5(a), the c_0 corresponding to the significant decrease of the W_c agrees with that corresponding to the marked increase of the c_i for each GB studied here. It may be shown that the W_c depends strongly on the hydrogen concentration c_i aggregated in the GBs, and the work of GB separation degrades as the c_i in each GB increases. In addition, the W_c of twin GB $\Sigma 3(110)[111]$ starts to significantly decrease until the c_0 is about 1×10^{-5} . It shows that the W_c of twin GB $\Sigma 3(110)[111]$ is the least sensitive to the equilibrium hydrogen concentration c_0 in bulk. That is, twin GB $\Sigma 3(110)[111]$ is the most resistant to hydrogen-induced intergranular fractures among all GBs studied here in the same hydrogen environment.

The decrease in GB separation work due to hydrogen segregation represented by the Rice-Wang model is a result based on the assumption that the amount of hydrogen segregation does not change during fracture surface formation. Therefore, this model does not consider the effect that hydrogen moves to the fracture surface during the formation of the fracture surface. The Rice-Wang model only works on the case of the GB fast fracture. However, as the GB fracture occurs at a low speed rather than at high speed, the hydrogen diffusion to fracture surfaces may happen, which will further reduce the separation work of the GBs. This has been demonstrated in other hydrogen-metal systems and called the mobile or chemo-mechanical effect of hydrogen [51–53]. To further consider the mobile effect of hydrogen in tungsten GBs, the equation (3) is simply rewritten as

$$W_c \approx W_0 - \sum_i (E_{GB,H}^{seg,i} * c_{i,GB} - E_{FS,H}^{seg,i} * c_{i,FS}) * \theta_i,$$

where $c_{i,GB}$ and $c_{i,FS}$ are respectively the hydrogen concentration in GB and fracture surface. According to this equation, taking GB $\Sigma 3(110)[111]$ as an example, the

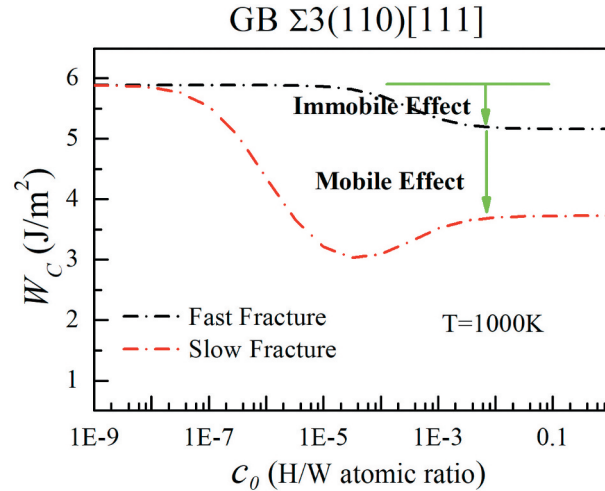


Figure 6. Comparison of the separation work W_0 of GB $\Sigma 3(110)[111]$ caused by only the immobile effect of hydrogen (fast fracture), and both of the mobile and immobile effects of hydrogen (slow fracture) with increasing bulk hydrogen concentration c_0 at 1000 K.

mobile effect of hydrogen was investigated. Figure 6 shows the comparison of the separation work W_c of GB $\Sigma 3(110)[111]$ caused by only the immobile effect of hydrogen (fast fracture), and both of the mobile and immobile effects of hydrogen (slow fracture) at 1000 K. Clearly, the hydrogen diffusion to fracture surface further decrease the separation work of GB $\Sigma 3(110)[111]$. In addition, compared to the fast fracture the separation work starts to decrease at lower c_0 for the slow fracture. For other GBs, the results are similar.

4. Discussion

One used charge density [13] and the volume distortion [54] to describe the interstitial sites. As shown in Figure 4, however, a new phenomenon was observed in this study, which was that the final distance between the H atom and its nearest W atom would become about 1.95 Å in interstitial sites (with hard-sphere radius r_0 larger than 0.57 Å, which was corresponding to the H-W distance of 1.95 Å) because H atom moved towards one of its neighboring atoms. Therefore, we inferred that there was an equilibrium H-W distance of 1.95 Å and the hard-sphere radius r_0 was employed to characterize the interstitial sites in this study.

Our calculations have shown that the larger the interstitial site in GB is, the higher the hydrogen concentration in the interstitial site is, the higher the hydrogen concentration in the GB is, and the smaller the work of the GB separation is. Therefore, this kind of GB with smaller interstitial sites is more resistant to the hydrogen segregations and the hydrogen-induced intergranular fractures. Among all the GBs studied here, the twin GB $\Sigma 3(110)[111]$ is the most resistant to the hydrogen segregations and the hydrogen-

induced intergranular fractures. Unfortunately, we do not find related experimental results in W so far. But the experimental results in nickel show that there are some ‘special GBs’ in nickel indeed enhancing the resistance to hydrogen-induced intergranular fractures [6]. Those ‘special GBs’ are generally of low excess free volume and high degree of atomic matching, and consist mainly of twin GB $\Sigma 3$ [6].

As PFM in fusion reactor, W will be exposed to H isotope (deuterium-tritium) ions, He ions as well as neutrons, which result in the presence of a larger number of vacancies and hydrogen atoms in W at the same time. It is well known that H atoms gather in the vacancies to form hydrogen bubble nucleus, and then the hydrogen bubble nucleus further grow by further capturing the vacancies and hydrogen atoms. Our previous study has also indicated that the twin GB $\Sigma 3(110)[111]$ has also the weakest trapping ability for vacancy in W compared to other GBs [31]. Therefore, the twin GB $\Sigma 3(110)[111]$ is also the most resistant to the hydrogen bubble nucleus and growth since it has the weakest trapping abilities for all of the vacancies and hydrogen atoms.

5. Conclusions

In this study, the H solubility and segregation in eight symmetric tilt GBs in W have been investigated through first-principles calculations. An equilibrium distance, about 1.95 Å, between H inserted in an interstitial site and its nearest W is discovered. The interactions between the inserted H and GBs are rather localized; thus, the hydrogen solubility is related to the local structures of the interstitial sites. It is found out that the hydrogen solution energy decreases as the hard-sphere radius r_0 of interstitial site increases, and the trend significantly slows down as the r_0 is more than 0.57 Å. This can be attributed to the fact that the contributions from lattice distortions induced by the inserted H to hydrogen solution energy can be ignored in these cases. In addition, the GBs with smaller interstitial site are more resistant to hydrogen segregation as well as hydrogen-induced intergranular fractures. Because the twin GB $\Sigma 3(110)[111]$ has the smallest interstitial site among GBs studied here, it has the weakest capability to trap H and it is the most resistant to hydrogen-induced intergranular fractures.

Disclosure statement

No potential conflict of interest was reported by the authors.

Funding

This work was supported by the National Natural Science Foundation of China [11775102,11805088]; Fundamental

Research Funds for the Central Universities [Izujbky-2018-19].

References

- [1] Ullmaier H. The influence of helium on the bulk properties of fusion reactor structural materials. *Nucl Fusion*. 1984;24(8):1039.
- [2] Trinkaus H, Singh BN. Helium accumulation in metals during irradiation—where do we stand. *J Nucl Mater*. 2003;323(2–3):229–242.
- [3] Lassila DH, Birnbaum HK. The effect of diffusive hydrogen segregation on fracture of polycrystalline nickel. *Acta Metall*. 1986;34(7):1237.
- [4] Thomas RLS, Scully JR, Gangloff RP. Internal hydrogen embrittlement of ultrahigh-strength AERMET 100 steel. *Metall Mater Trans A*. 2003;34(2):327–344.
- [5] Lee Y, Gangloff RP. Measurement and modeling of hydrogen environment-assisted cracking of ultra-high-strength steel. *Metall Mater Trans A*. 2007;38(13):2174.
- [6] Bechtle S, Kumar M, Somerday BP, et al. Grain-boundary engineering markedly reduces susceptibility to intergranular hydrogen embrittlement in metallic materials. *Acta Mater*. 2009;57(14):4148..
- [7] Yu Y, Shu X, Liu Y, et al. Molecular dynamics simulation of hydrogen dissolution and diffusion in a tungsten grain boundary. *J Nucl Mater*. 2014;455(1–3):91–95..
- [8] Hodille EA, Ghiorgiu F, Addab Y, et al. Retention and release of hydrogen isotopes in tungsten plasma-facing components: the role of grain boundaries and the native oxide layer from a joint experiment-simulation integrated approach. *Nucl Fusion*. 2017;57(7):076019..
- [9] Zhao Z, Li Y, Zhang C, et al. Effect of grain size on the behavior of hydrogen/helium retention in tungsten: a cluster dynamics modeling. *Nucl Fusion*. 2017;57(8):086020..
- [10] Valles G, Panizo-Laiz M, González C, et al. Influence of grain boundaries on the radiation-induced defects and hydrogen in nanostructured and coarse-grained tungsten. *Acta Mater*. 2017;122:277–286.
- [11] He Z, He HY, Chen JL, et al. Accumulation of beryllium and its effects on hydrogen retention in tungsten divertor. *Nucl Fusion*. 2018;58(10):106015..
- [12] Pundt A, Kirchheim R. Hydrogen in metals: microstructural aspects. *Ann Rev Mater Res*. 2006;36(1):555–608.
- [13] Zhou HB, Liu YL, Jin S, et al. Investigating behaviours of hydrogen in a tungsten grain boundary by first principles: from dissolution and diffusion to a trapping mechanism. *Nucl Fusion*. 2010;50(2):025016..
- [14] Xiao W, Geng WT. Role of grain boundary and dislocation loop in H blistering in W: A density functional theory assessment. *J Nucl Mater*. 2012;430(1–3):132–136.
- [15] Piaggi PM, Bringa EM, Pasianot RC, et al. Hydrogen diffusion and trapping in nanocrystalline tungsten. *J Nucl Mater*. 2015;458:233.
- [16] González C, Panizo-Laiz M, Gordillo N, et al. H trapping and mobility in nanostructured tungsten grain boundaries: a combined experimental and theoretical approach. *Nucl Fusion*. 2015;55(11):113009..

- [17] Oudriss A, Creus J, Bouhattate J, et al. The diffusion and trapping of hydrogen along the grain boundaries in polycrystalline nickel. *Scr Mater.* **2012**;66(1):37.. .
- [18] Kaufmann M, Neu R. Tungsten as first wall material in fusion devices. *Fusion Eng Des.* **2007**;82(5–14):521.
- [19] Zinkle SJ. Fusion materials science: overview of challenges and recent progress. *Phys Plasmas.* **2005**;12 (5):058101.
- [20] Troiano AR. The role of hydrogen and other interstitials in the mechanical behavior of metals. *Trans Am Soc Met.* **1960**;52:54.
- [21] Goto J, Ohsawa K, Yagi M. Numerical study on hydrogen retention at a grain boundary in tungsten. *Rep Res Inst App Mec Kyushu Univ.* **2010**;139:75–79.
- [22] Grimmer H. Coincidence-site lattices. *Acta Crystallogr Sect A.* **1976**;32(5):783.. .
- [23] Perdew JP, Burke K, Ernzerhof M. Generalized gradient approximation made simple. *Phys Rev Lett.* **1996**;77(18):3865.
- [24] Kresse G, Hafner J. Ab initio molecular dynamics for liquid metals. *Phys Rev B.* **1993**;47(1):558.
- [25] Kresse G, Furthmuller J. Efficiency of ab-initio total energy calculations for metals and semiconductors using a plane-wave basis set. *Comput Mater Sci.* **1996**;6(1):15–50.
- [26] Kresse G, Furthmuller J. Efficient iterative schemes for ab initio total-energy calculations using a plane-wave basis set. *Phys Rev B.* **1996**;54(16):11169.
- [27] Hohenberg P, Kohn W. Inhomogeneous electron gas. *Phys Rev B.* **1964**;136(3B):864.
- [28] Gonze X, Ghosez P, Godby RW. Density-functional theory of polar insulators. *Phys Rev Lett.* **1997**;78(2):294.
- [29] Perdew JP, Wang Y. Accurate and simple analytic representation of the electron-gas correlation energy. *Phys Rev B.* **1992**;45(23):13244.
- [30] He WH, Gao X, Wang D, et al. First-principles investigation of grain boundary morphology effects on helium solutions in tungsten. *Comput Mater Sci.* **2018**;148:224–230.
- [31] He WH, Gao X, Gao N, et al. Effects of grain boundary characteristics on its capability to trap point defects in tungsten. *Chin Phys Lett.* **2018**;35(2):026101.. .
- [32] Yamaguchi M. First-principles study on the grain boundary embrittlement of metals by solute segregation: part I. Iron (Fe)-Solute (B, C, P, and S) Systems. *Metall Mater Trans A.* **2011**;42(2):319–329.
- [33] Tian Z, Yan J, Xiao W, et al. Effect of lateral contraction and magnetism on the energy release upon fracture in metals: first-principles computational tensile tests. *Phys Rev B.* **2009**;79(14):144114.. .
- [34] Rice JR, Wang JS. Embrittlement of interfaces by solute segregation. *Mater Sci Eng A.* **1989**;107:23–40.
- [35] Liu YL, Zhang Y, Luo GN, et al. Structure, stability and diffusion of hydrogen in tungsten: A first-principles study. *J Nucl Mater.* **2009**;390–391:1032–1034.
- [36] Liu YL, Zhang Y, Zhou HB, et al. Vacancy trapping mechanism for hydrogen bubble formation in metal. *Phys Rev B.* **2009**;79(17):172103.. .
- [37] Duan C, Liu YL, Zhou HB, et al. First-principles study on dissolution and diffusion properties of hydrogen in molybdenum. *J Nucl Mater.* **2010**;404(2):109–115.. .
- [38] Du YA, Ismer L, Rogal J, et al. First-principles study on the interaction of H interstitials with grain boundaries in α - and γ -Fe. *Phys Rev B.* **2011**;84(14):144121.. .
- [39] Song J, Curtin WA. A nanoscale mechanism of hydrogen embrittlement in metals. *Acta Mater.* **2011**;59(4):1557–1569.
- [40] Song J, Curtin WA. Atomic mechanism and prediction of hydrogen embrittlement in iron. *Nat Mater.* **2013**;12(2):145–151.
- [41] Seletskaia T, Ossetsky Y, Stoller RE, et al. Magnetic interactions influence the properties of helium defects in iron. *Phys Rev Lett.* **2005**;94(4):046403.. .
- [42] Zhou HB, Wang JL, Jiang W, et al. Electrophobic interaction induced impurity clustering in metals. *Acta Mater.* **2016**;119:1–8.
- [43] Zhou HB, Jin S, Zhang Y, et al. Anisotropic strain enhanced hydrogen solubility in bcc metals: the independence on the sign of strain. *Phys Rev Lett.* **2012**;109(13):135502.. .
- [44] Wu R, Freeman AJ, Olson GB. First principles determination of the effects of phosphorus and boron on iron grain boundary cohesion. *Sci.* **1994**;265 (5170):376.
- [45] Li YH, Zhou HB, Jin S, et al. Strain-induced variation of electronic structure of helium in tungsten and its effects on dissolution and diffusion. *Comput Mater Sci.* **2014**;95:536–539.
- [46] Ferrin P, Kandoi S, Nilekar AU, et al. Hydrogen adsorption, absorption and diffusion on and in transition metal surfaces: a DFT study. *Surf Sci.* **2012**;606 (7–8):679–689.. .
- [47] Christmann K. Interaction of hydrogen with solid surfaces. *Surf Sci Rep.* **1988**;9(1–3):1.
- [48] Setyawan W, Kurtz RJ. Ab initio study of H, He, Li and Be impurity effect in tungsten 3{112} and 27 {552} grain boundaries. *J Phys Condens Matter.* **2014**;26(13):135004.
- [49] Wright GM, Alves E, Alves LC, et al. Hydrogen retention of high-Z refractory metals exposed to ITER divertor-relevant plasma conditions. *Nucl Fusion.* **2010**;50(5):055004.
- [50] Wu X, You Y, Kong X, et al. First-principles determination of grain boundary strengthening in tungsten: dependence on grain boundary structure and metallic radius of solute. *Acta Mater.* **2016**;120:315–326.
- [51] Yamaguchi M, Kameda J, Ebihara KI, et al. Mobile effect of hydrogen on intergranular decohesion of iron: first-principles calculations. *Phil Mag.* **2012**;92 (11):1349–1368.. .
- [52] Kirchheim R, Somerday B, Sofronis P. Chemomechanical effects on the separation of interfaces occurring during fracture with emphasis on the hydrogen-iron and hydrogen-nickel system. *Acta Mater.* **2015**;99:87–98.
- [53] Wang S, Martin ML, Robertson IM, et al. Effect of hydrogen environment on the separation of Fe grain boundaries. *Acta Mater.* **2016**;107:279–288.
- [54] Zhou X, Marchand D, McDowell DL, et al. chemo-mechanical origin of hydrogen trapping at grain boundaries in fcc metals. *Phys Rev Lett.* **2016**;116 (7):075502.